ChemComm

Phase Transition of Spiropyrans: Impact of Isomerization Dynamics at High Temperatures

Journal:	*ChemComm*
Manuscript ID	CC-COM-03-2019-002141.R1
Article Type:	Communication

COMMUNICATION

Phase Transition of Spiropyrans: Impact of Isomerization Dynamics at High Temperatures

Received 00th January 20xx,
Accepted 00th January 20xx

DOI: 10.1039/x0xx00000x

Mihael A. Gerkman, Shichen Yuan, Pu Duan, Jennifer Taufan, Klaus Schmidt-Rohr, and Grace G. D. Han*

Isomerization behaviors of spiropyran derivatives in neat condensed phase were studied to understand their unusual phase transitions including cold-crystallization after extreme supercooling down to −50 °C. Compounds with different functional groups were compared, and the equilibrium between isomers at high temperatures was found to determine phase transitions.

Molecules that change their conformation upon exposure to external stimuli have been of interest to diverse fields of study and applications such as sensing,[1] drug delivery,[2] and memory[3] due to the rapid and significant changes of their physical properties.[4] Diverse molecules have been designed and further tailored to enhance their response to a specific stimulus, such as light,[5] heat,[6] current,[7] pH,[8] metal ions,[9] or toxic gases.[10] Molecules that exhibit a reversible response to a stimulus by isomerization are of particular interest since they enable repeated operation. Molecules with a significant color change during the reversible isomerization, such as spiropyran,[11] diarylethene,[12] and donor-acceptor Stenhouse adduct,[13] have been widely explored for developing chromic sensors.

The fundamental understanding of the chromic isomerization is generally achieved by solution-state nuclear magnetic resonance (NMR) and UV-Visible absorption spectroscopy (UV-Vis), which monitor the relative population of isomers in the solution mixtures. Thermochromic,[14] photochromic,[15] solvatochromic,[16] acidochromic,[17] and electrochromic[18] behaviors of diverse molecules have been primarily investigated in dilute solution, where unhindered structural changes are promoted by solvation. Isomerization of molecules dispersed in polymers,[19] hydrogels,[20] and other soft matrices[21] including liquid crystals[22] that allow for the structural changes has also been widely investigated for solid-state applications (Fig. 1a).

The study of molecular isomerization in solid or liquid 'neat' phase (*i.e.* pristine molecules without any solvent or matrix), however, has been rather limited as the result of difficulties in achieving structural changes due to the close packing of molecules in the solid state or high temperature required to reach the molten state. At temperatures far above ambient, the energy input from the surroundings creates a new equilibrium of isomerization. Exploring a melt state of isomerizing molecules at a temperature close to 200 °C can provide new insights into thermodynamically-driven isomerization in condensed phase, which is drastically different from the isomerization dynamics at room temperature in solution. In the 1980s, Krongauz and coworkers presented remarkable studies of spiropyrans functionalized with mesogenic groups forming quasi-liquid crystals at elevated temperatures (50-130 °C), but the focus was on the observation of birefringence from solution-cast metastable films.[23]

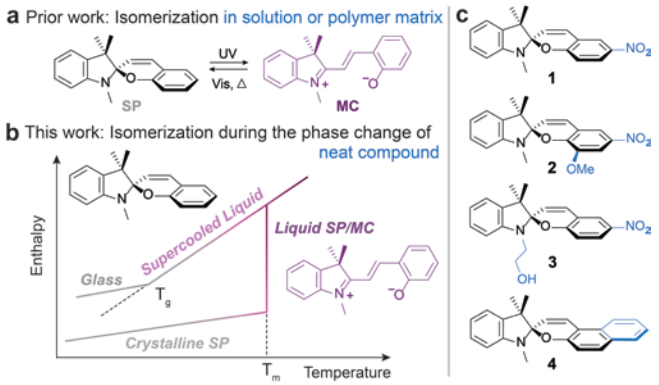

Fig. 1 (a) Isomerization between spiropyran (SP) and merocyanine (MC) forms, occurring in solvated or dispersed conditions. (b) Energy diagram of phase transition and simultaneous isomerization of SP during initial melting and subsequent cooling below the melting point (T_m). The supercooled liquid becomes an amorphous solid below the glass transition point (T_g). (c) Four SP derivatives among eight compounds studied in this work. Compounds **5**-**8** are shown in Fig. S1. Functional groups are highlighted in blue.

As shown in Fig. 1b, unique phase behavior of pristine molecules such as supercooling is observed. Insights into the molecular isomerization dynamics in condensed phase can open up new opportunities in developing stimulus-responsive solid-state applications, such as memories, sensors, actuators, and removable adhesives, which should consist of bulk materials without solvation. The processing of such bulk

Department of Chemistry, Brandeis University, 415 South Street, Waltham, MA 02453, USA.
E-mail: gracehan@brandeis.edu
† Electronic Supplementary Information (ESI) available.
See DOI: 10.1039/x0xx00000x

materials often involves thermal treatment to achieve a desired arrangement of molecules and morphology of films.[24]

In this study, we explore how spiropyran (SP)-merocyanine (MC) isomers undergo unique phase transitions that are closely linked to their isomerization dynamics. We studied diverse spiropyran derivatives and successfully characterized the condensed-phase isomerization dynamics of four compounds **1**-**4** (Fig. 1c). A nitro group at the 6-position of benzopyran moiety is known to shift the equilibrium toward open isomeric forms in solutions,[25] and such behavior in condensed phase was studied. The equilibrium constant is also known to increase with solvent polarity,[26] and we varied the polarity of substituents on 1- or 8-position to imitate the solvent effect which was translated as spiropyran matrix effect in condensed phase. Compound **4** was selected since spironaphthopyrans were reported to possess significant quantum yields of switching (0.2-0.9) in solutions.[27] In Supporting Note 1 and Fig. S1, we elaborate the results of other derivatives without a nitro group (compounds **5**-**8**), which were inconclusive due to thermal decomposition, low MC concentration, and limited photoswitching.

Fig. 2 summarizes the phase transitions of SP derivatives **1**-**4**. During initial heating up to 180–210 °C, all crystalline SP compounds (**1**-**4**) show endothermic peaks (red shading) that correspond to melting at around 170–180 °C, but the molten phase of SP compounds behaves differently upon subsequent cooling (Fig. 2a,b,c,g,h). Only compound **1** readily crystallizes above 120 °C, while compounds **2**-**4** do not exhibit exothermic crystallization on differential scanning calorimetry (DSC) even after cooling down to −50 °C. Instead, compounds **2**-**4** undergo glass transitions at 44-58 °C, forming an amorphous solid (glass) at room temperature. Compound **4**, in particular, shows an intriguing cold-crystallization behavior when the supercooled glass is heated from −50 °C to 112 °C (Fig. 2g). The cold-crystallization is not observed if the supercooling is stopped at temperatures above −35 °C (Fig. 2h). We note that thermal decomposition of compounds is negligible, as shown by the unchanged NMR spectra of compounds obtained after repeated DSC cycles (Fig. S2 and S3). Thermogravimetric analysis (TGA) is also provided to confirm the thermal stability of compounds **1**-**4** (Fig. S4). We also confirmed the identical thermal behaviors of the compounds measured at varied rates (10 and 2 °C/min) as shown in Fig. S5. The temperature and enthalpy involved in each transition were recorded and presented in Table S1.

During these thermal cycles, initially crystalline compounds **1**-**4** show darker and more vivid color in their molten phase (Fig. 2d,e,f,i), which indicates the increased population of the conjugated MC isomers at high temperatures. As the molten compounds are cooled and crystalline or amorphous solids form, the color turns lighter, which indicates a decreased MC content. X-ray diffraction (XRD) measurement (Fig. 2j-l) corroborates the DSC results and visual observations; initially crystalline SP derivatives show strong diffraction patterns (black lines). Except for compound **1**, which immediately crystallizes after melting and cooling, other compounds (**2**-**4**) form an amorphous solid phase after melting and cooling, supported by the absence of diffraction peaks (blue lines). Interestingly, amorphous compound **4** starts to exhibit diffraction peaks only

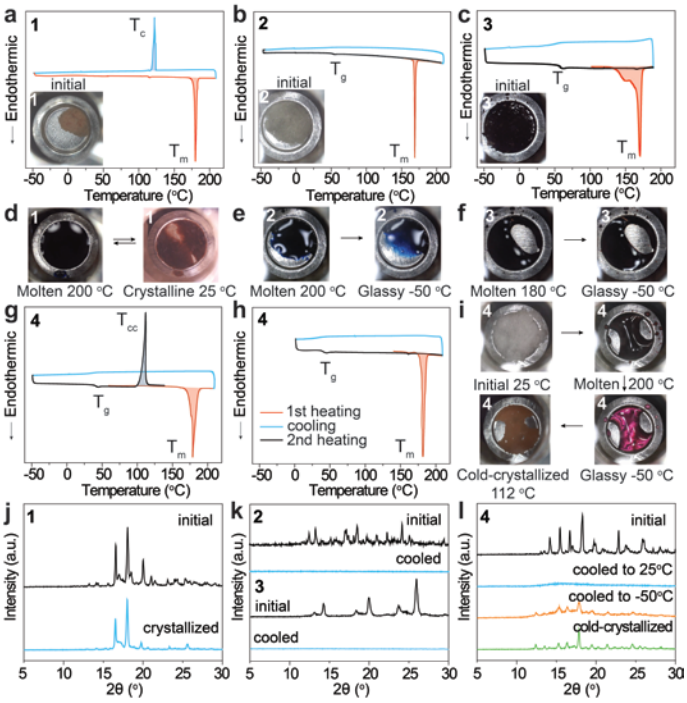

Fig. 2 DSC curves of (a) compound **1**, (b) **2**, and (c) **3**. Insets are low magnification optical microscope images (5x5 mm) of initial crystalline powder. Images of (d) **1**, (e) **2**, (f) **3** taken during heating and cooling cycles of DSC. DSC curves of compound **4** (g-h) being first melted (red curve), subsequently cooled (blue curve), then re-heated (black curve). Cold crystallization of **4** was not observed when the molten compound was cooled to 0 °C as shown in (h). T_m: melting point, T_c: crystallization point, T_g: glass transition point, T_{cc}: cold-crystallization point, Shaded areas integrate to yield the specific enthalpy (in J/g) for each phase transition. (i) Images of **4** taken during heating and cooling cycles of DSC, showing relevant phase transitions. XRD patterns of (j) **1**, (k) **2** and **3**, and (l) **4** at initial crystalline state and after heating and cooling cycles.

upon further cooling to −50 °C, and the peaks become more pronounced after the cold-crystallization at 112 °C. This indicates that compound **4** forms small crystalline nucleation seeds when cooled to −50 °C, which induces cold-crystallization upon subsequent heating. This seed formation is not observed in compound **2** and **3**. The crystal structures of compound **1**, **3**, and **4** (Fig. S6) as spiropyran and merocyanine forms show distinct structural differences and intermolecular packing in solid state. Also, drastically different dipole moments of the SP (~4-6 D) and MC form (~14-18 D)[11] indicate that thermally generated MC isomers in SP matrix during the melting process exerts a significant effect on SP packing and phase transition.

In order to assess the impact of SP-MC isomerization on the different phase transitions, we measured the relative concentration of each isomer in condensed phase at room temperature as well as high temperatures during the melting-cooling process. First, a quantitative solid-state ^{13}C NMR spectrum of melt-cooled compound **2** was taken at room temperature (Fig. 3a), which confirmed its amorphous nature by displaying peaks significantly broadened compared to those of pristine crystalline compound **2** (Fig. S7). Surprisingly, most of the observed chemical shifts corresponded to those of SP. The concentration of MC was low as indicated by the small intensity of the characteristic MC peaks near 180 ppm from the non-protonated carbon atoms that are double-bonded to O and N in the MC resonance structures (Fig. 3a inset). The combined

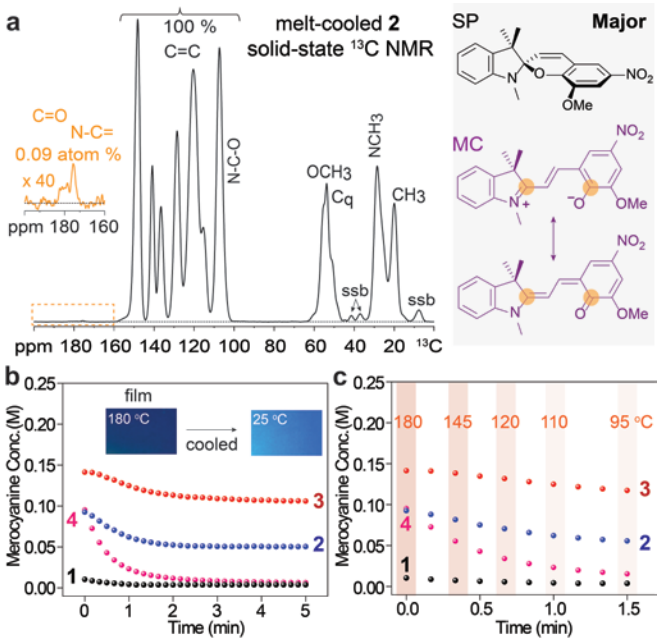

Fig. 3 (a) Solid-state ^{13}C NMR spectrum of melt-cooled compound **2** at room temperature. The inset on the left shows the signals at >160 ppm after 40-fold vertical scaling. The two peaks observed correspond to 0.7 ± 0.2 wt% of the MC isomer. "ssb": spinning sideband. (b) Change of MC concentration (solution-NMR-calibrated), from absorbance at 550-600 nm, in neat films of compounds **1**-**4** during the spontaneous cooling under ambient condition, once heated above the T_m. After 5 min, the films reach room temperatures. (inset) Digital photograph of the film of compound **2** during this cooling process. (c) Initial change of MC concentration measured during 1.5 min. Temperature change was measured by an IR thermometer (Fig. S8).

peak intensity is 0.09% relative to SP peaks at 100-150 ppm, which corresponds to 0.7 ± 0.2 wt% of MC in the solid. We confirmed this analysis of MC concentration in amorphous compound **2** by performing a comparative UV-Vis measurement of amorphous films (around 5 μm thick) and solutions (1 and 0.01 mg/mL in DMSO-d^6) whose MC content was measured by ^1H NMR (Fig. S9). Assuming the same molar extinction coefficient (Ɛ at around 600 nm) of MC isomer in solution and in SP solid matrix, we obtained around 1 wt% MC (0.05 M) in the amorphous solid, in agreement with the result of solid-state NMR. The amorphous solid of compound **2** is still vividly colored as seen in Fig. 2e, and the UV-Vis of the film also shows strong absorption around 500-700 nm due to the high Ɛ value (Fig. S10).

Given this low MC content in the mixture, we speculated that the MC-to-SP conversion during the cooling of the molten compound occurs rapidly and may differently impact the crystallization of each molten compound. Fig. 3b shows the MC concentration changing in neat films during spontaneous cooling immediately after melting. The UV-Vis spectra of heated films were first obtained (Fig. S10), then the absorbance change was converted to concentration change by applying the Ɛ measured in solution and calibrated by solution NMR (Fig. S11) and the film thickness measured by a profilometer (Table S2). Analogous to solution-state behavior, compounds **1**-**4** display significantly different MC concentration profiles in condensed phase for this cooling process. In detail, the measurements within the first 1.5 min (Fig. 3c) indicate that compound **1** possesses extremely low MC content even at high temperatures (0.1 wt% at 120 °C), while the other compounds maintain higher concentrations of MC especially above 120 °C (1.4 wt% for compound **2**, 2.6 wt% for compound **3**, and 0.7 wt% for compound **4** at 120 °C). This signifies the role of MC isomers in preventing SP crystallization, acting as minor dopants, since only compound **1** crystallizes above 120 °C whereas other compounds with higher MC content remain amorphous even after cooling to −50 °C (Fig. 2). Furthermore, compound **4**, which cold-crystallizes after supercooling, exhibits a continuously decreasing MC content to 0.13 wt% at room temperature nearly identical to that of compound **1** (0.08 wt%). MC isomers of compound **3**, produced during melting, formed H-aggregates as the film was cooled to room temperature, showing a blue shift of absorbance (Fig. S10c). MC concentration was evaluated by the absorbance change at 590 nm, consistent to the method used for compounds **1** and **2**, but the overall decrease of the MC isomer **3** was minimal. The high MC content of melted compound **3** indicates that factors impacting the SP-MC equilibrium in condensed phase are analogous to those in solution state.

Based on these observations, we have summarized the results in Fig. 4. When heated above the melting point, SP compounds thermally isomerize to entropy-favored MC forms to different degrees; compound **1** has a lower SP-to-MC conversion than compounds **2**-**4**. Once liquefied then cooled down, the MC-to-SP reversion takes place. Compound **1** with an initially low MC content readily crystallizes due to the negligible dopant effect. Compounds **2**-**4**, on the other hand, contain significant MC dopants. Due to their very different molecular structure, the MC dopants, despite making up as little as around 1 wt% of the mixture, effectively disturb the ordering of mobile SP molecules, thus stabilizing the glassy phase. Compound **4** experiences further loss of the MC form upon cooling to −50 °C and thus develops the local crystalline packing of SP molecules or "nucleation seeds" (Fig. 2l and Fig. S7a) that enable cold-crystallization when thermal energy is provided.

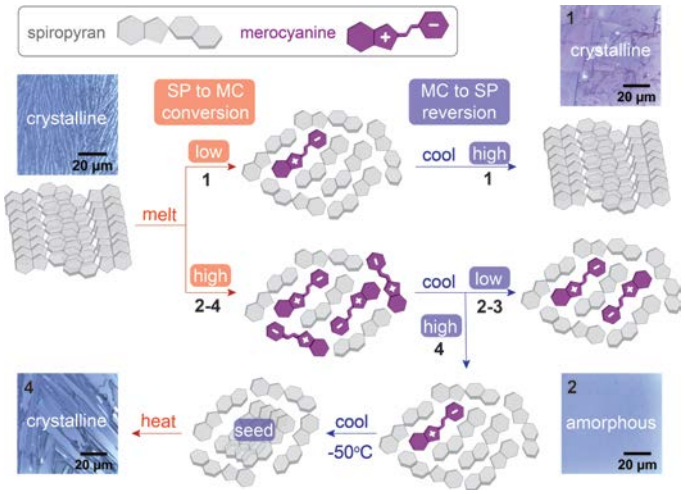

Fig. 4 Schematic illustration of the phase change of compounds **1**-**4**. High magnification optical microscope images show the morphology of thin film samples at each stage. Depending on the relative SP and MC content (illustrative, not quantitative presentation), the crystallinity of melt-cooled compound is determined, as minor MC plays a role as a dopant that prevents crystallization of liquid phase.

We speculate that the intrinsic equilibrium between SP and MC isomers of each compound in a condensed SP-rich system above T_g impacts the phase transition. Thus, we further investigated the kinetics of MC-to-SP isomerization in a relatively non-polar and mobile medium (*i.e.* toluene solution) by first photo-saturating MC isomers then observing the MC decays at various temperatures (20, 40, and 60 °C) in the dark (Fig. S12 and S13). The kinetic constants (k) of MC-to-SP conversion for compounds **1**, **2**, and **3** were obtained (Table S3), for example, 0.045, 0.020, and 0.002 sec^{-1} at 20 °C, respectively. This confirms that the isomerization equilibrium favors SP saturation in the following order: compound **1**>**2**>**3**, which is consistent with the results of our thin-film studies (Fig. 3b). The isomerization of compound **4** was challenging in various organic solutions (Fig. S12) due to the low activation energy for the thermal reversion (MC to SP) in such condition, thus its k value is not reported here.

Lastly, the application of the melt-cooled compounds as optical memory was demonstrated (Fig. 5). The amorphous films (compounds **2**-**4**) generated by the simple melt-cooling process are an effective platform for optical switching and information storage, due to the photoswitching capability of SP molecules. A pattern on a film that is exposed to UV (365 nm) becomes darker as the MC content increases (Fig. 5a-c). The film of compound **4** at room temperature is rapidly depleted of MC content (Fig. 3b), showing very light color. The contrast of the pattern is not as significant as that of compound **2** or **3**. The patterns are maintained for weeks under ambient conditions and removed only by the simultaneous heating above T_g and strong visible light irradiation, which triggers MC-to-SP reversion in the relatively mobile solid state. The crystalline film of compound **1**, on the other hand, was found to be difficult to pattern with clear images, as a result of the constrained molecular packing in the crystalline phase (Fig. 5d). We conclude that spiropyran derivatives with 6-nitro group and additional polar substituents, which generate and retain significant MC content through melting and amorphization process, are optimal for optical memory applications. The long storage time and the specific triggering mechanism for restoration are desired characteristics for effective optical memory,[28] and further studies of this unique property of neat amorphous solids and their viability for applications are currently being pursued.

We gratefully acknowledge the support from NSF (Award No. 1726346) for the solid-state NMR spectrometer.

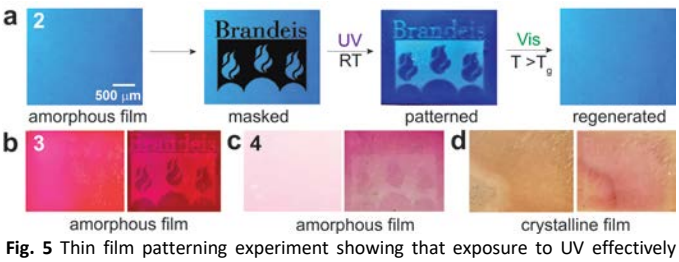

Fig. 5 Thin film patterning experiment showing that exposure to UV effectively isomerizes SP molecules in the amorphous solid of compound (a) **2**, (b) **3**, and (c) **4**. (d) Crystalline film of compound **1** showing difficulty of patterning and crystalline features.

Conflicts of interest

There are no conflicts to declare.

Notes and references

1 I. S. Park, Y. S. Jung, K. J. Lee and J. M. Kim, *Chem. Commun.*, 2010, **46**, 2859-2861.
2 T. Senthilkumar, L. Zhou, Q. Gu, L. Liu, F. Lv and S. Wang, *Angew. Chem., Int. Ed.*, 2018, ***57***, 13114-13119.
3 M. Berberich, A. M. Krause, M. Orlandi, F. Scandola and F. Würthner, *Angew. Chem., Int. Ed.*, 2008, **47**, 6616-6619.
4 M. Natali and S. Giordani, *Chem. Soc. Rev.*, 2012, **41**, 4010-4029.
5 A. S. Lubbe, C. Böhmer, F. Tosi, W. Szymanski and B. L. Feringa, *J. Org. Chem.*, 2018, **83**, 11008-11018.
6 H. Wang, H. K. Bisoyi, L. Wang, A. M. Urbas, T. J. Bunning and Q. Li, *Angew. Chem., Int. Ed.*, 2018, **57**, 1627-1631.
7 J. Sun, Y. Wu, Y. Wang, Z. Liu, C. Cheng, K. J. Hartlieb, M. R. Wasielewski and J. F. Stoddart, *J. Am. Chem. Soc.*, 2015, **137**, 13484-13487.
8 P. K. Kundu, G. L. Olsen, V. Kiss and R. Klajn, *Nat. Commun.*, 2014, **5**, 3588.
9 Y. Ren, P. H. Svensson and O. Ramström, *Angew. Chem., Int. Ed.*, 2018, **57**, 6256-6260.
10 J. W. Lee and R. Klajn, *Chem. Commun.*, 2015, **51**, 2036-2039.
11 R. Klajn, *Chem. Soc. Rev.*, 2014, **43**, 148-184.
12 M. Irie, T. Fukaminato, K. Matsuda and S. Kobatake, *Chem. Rev.*, 2014, **114**, 12174-12277.
13 (a) M. M. Lerch, W. Szymański and B. L. Feringa, *Chem. Soc. Rev.*, 2018, **47**, 1910-1937; (b) J. R. Hemmer, Z. A. Page, K. D. Clark, F. Stricker, N. D. Dolinski, C. J. Hawker and J. Read de Alaniz, *J. Am. Chem., Soc.*, 2018, **140**, 10425-10429.
14 Y. Liu, A. H. Flood and J. F. Stoddart, *J. Am. Chem. Soc.*, 2004, **126**, 9150-9151.
15 D. Samanta, J. Gemen, Z. Chu, Y. Diskin-Posner, L. J. W. Shimon and R. Klajn, *Proc. Natl. Acad. Sci.*, 2018, **115**, 9379-9384
16 M. M. Lerch, M. Di Donato, A. D. Laurent, M. Medved, A. Iagatti, L. Bussotti, A. Lapini, W. J. Buma, P. Foggi, W. Szymański and B. L. Feringa, *Angew. Chem., Int. Ed.*, 2018, **57**, 8063-8068.
17 P. Remón, S. M. Li, M. Grøtli, U. Pischel and J. Andréasson, *Chem. Commun.*, 2016, **52**, 4659-4662.
18 R. Rathore, P. Le Magueres, S. V. Lindeman and J. K. Kochi, *Angew. Chem., Int. Ed.*, 2000, **39**, 809-812.
19 X. Fang, H. Zhang, Y. Chen, Y. Lin, Y. Xu and W. Weng, *Macromolecules*, 2013, **46**, 6566-6574.
20 X. Xiao, J. Hu, X. Wang, L. Huang, Y. Chen, W. Wang, J. Li and Y. Zhang, *Chem. Commun.*, 2016, **52**, 12517-12520.
21 A. Julià-López, J. Hernando, D. Ruiz-Molina, P. González-Monje, J. Sedó and C. Roscini, *Angew. Chem., Int. Ed.*, 2016, **55**, 15044-15048.
22 M. M. Russew and S. Hecht, *Adv. Mater.* 2010, **22**, 3348-3360.
23 (a) F. P. Shvartsman and V. A. Krongauz, *J. Phys. Chem.*, 1984, **88**, 6448-6453; (b) F. Shvartsman and V. Krongauz, *Nature*, 1984, **309**, 608-611.
24 Q. Yu, X. Su, T. Zhang, Y. M. Zhang, M. Li, Y. Liu and S. X. A. Zhang, *J. Mater. Chem. C*, 2018, **6**, 2113-2122.
25 X. Song, J. Zhou, Y. Li, and Y. Tang, *J. Photochem. Photobiol., A*, 1995, **92**, 99-103.
26 A. K. Chibisov and H. Görner, *J. Phys. Chem. A*, 1997, **101**, 4305-4312.
27 A. Kellman and F. Tfibel, *J. Photochem. Photobiol., A*, 1993, **76**, 77-82.
28 X. Liu, X. Jia, M. Fischer, Z. Huang and D. R. Smith, *Nano Lett.*, 2018, **18**, 6181-6187.